


Article

The Enhancement of H₂ Evolution over Sr_{1–1.5x}Tb_xWO₄ Solid Solution under Ultraviolet Light Irradiation

Jia Yang *, Xiaorui Sun *, Ting Zeng, Yilan Hu and Jianwei Shi

Chongqing Key Laboratory of Inorganic Special Functional Materials, College of Chemistry and Chemical Engineering, Yangtze Normal University, Fuling, Chongqing 408100, China; zengting@163.com (T.Z.); huyilan@163.com (Y.H.); shijianwei@163.com (J.S.)

* Correspondence: yangjiayznu@163.com (J.Y.); sunxiaoruiyynu@163.com (X.S.); Tel: +86-18716372096 (J.Y.); +86-18883876787 (X.S.)

Received: 3 April 2019; Accepted: 1 May 2019; Published: 8 May 2019



Abstract: In this work, Sr_{1–1.5x}Tb_xWO₄ (0 ≤ x ≤ 0.2) solid solutions were synthesized via a traditional high-temperature solid state method. Le Bail fitting on the powder X-ray diffraction (XRD) pattern showed that these solid solutions are pure phase. Scanning electron microscopy showed that the SrWO₄ and Sr_{0.82}Tb_{0.12}WO₄ samples are composed of micrometer particles and submicron crystallites, respectively. Ultraviolet–visible diffuse reflectance spectra suggested that the bandgaps of Sr_{1–1.5x}Tb_xWO₄ are narrower than the undoped sample. The Sr_{0.82}Tb_{0.12}WO₄ sample, with the assistance of 1.5 wt % Ru-cocatalyst, exhibits the best performance for H₂ evolution in 5 vol % aqueous triethanolamine (TEOA), which results in about 6.1 and 2.8 times efficiency improvement compared with the intrinsic SrWO₄ in methanol and aqueous TEOA, respectively. All the photocatalysts recycled after the photocatalytic reactions showed no degradation when checked by powder XRD.

Keywords: photocatalysis; semiconductor; solid solution; H₂ evolution; cocatalyst

1. Introduction

Photocatalytic technology is a green way to obtain clean energy hydrogen via semiconductor from water under sunlight irradiation [1]. Over the past few decades, various semiconducting materials, including oxide [2], sulfide [3], oxynitride [4], and carbon-based material [5], have been studied extensively in photocatalytic H₂ evolution. The sulfide and oxynitride materials generally have excellent photocatalytic activities, however, both of them are not stable enough in aqueous solution under light irradiation. For instance, the Zn_{1–2y}Ga_{1.7}In_{0.3}S₄ and Pt–PdS/CdS samples have outstanding photocatalytic H₂ evolution activities in aqueous S^{2–}/SO₃^{2–} solutions [6,7]. GaN/ZnO and LaMg_xTa_{1–x}O_{1+3x}N_{2–3x} solid solutions require a cocatalyst or coating material for photocatalytic H₂ evolution [8,9]. On account of their distinguished electrical conductivity, carbon materials have been utilized to fabricate carbon-based composites [10–12]. The majority of oxides were usually only sensitized by UV light, however, if suitable crystal structure can indicate good photocatalytic application [13,14].

The photocatalytic performance of SrWO₄ has been studied extensively in the field of environmental photocatalysis. Suitable SrWO₄ crystal structures are able to degrade various dyes and organic materials under ultraviolet light [15–21]. For example, rhodamine B and 6G were photodegraded by star-like SrWO₄ microcrystals in water [17]. The methyl orange degradation by SrWO₄ nanoparticles was about 73% after 60 min ultraviolet light illumination [20]. Ibuprofen was photoelectrooxidized by rice-like SrWO₄ nanocrystals in Na₂SO₄ solution [21]. In addition, there is a

single report of H₂ evolution by SrWO₄ micro/nanostructures in aqueous methanol under ultraviolet light irradiation [22]. However, the enhancement of H₂ evolution over SrWO₄ is lacking.

Generally, fabricating a solid solution is a powerful way to improve photocatalytic performance. For instance, the In_{1-x}Ni_xTaO₄ [2] and CuFe_{1-y}Cr_yS₂ [23] solid solutions were obtained as optimal samples for photocatalytic applications, where $x = 0.1$ and $y = 0.4$ in each solid solution. The enhancement of photocatalytic activity was due to the narrowing of the bandgap and the changing of the conduction band potential by the doped element [6]. Usually, the bandgap value and conduction band potential of photocatalyst are 1.23 eV and less than 0 V, respectively. In this paper, the photocatalytic H₂ evolution of scheelite structure SrWO₄ was improved by doping rare earth ions and cocatalysts. The Sr_{1-1.5x}Tb_xWO₄ solid solutions were studied for the first time in aqueous TEOA under ultraviolet light irradiation, and their photocatalytic activity was improved by loading various cocatalysts, such as Cu, Ag, Au, Pt, Ni, and Ru.

2. Materials and Methods

2.1. Preparations of the Catalysts

The solid state method was applied to synthesize Sr_{1-1.5x}Tb_xWO₄ ($0 \leq x \leq 0.2$) bulk samples. The starting materials, SrCO₃ (99.9%, Sinopharm Chemical Reagent Co., Ltd.), Tb₄O₇ (99.99%, Alfa Aesar), and WO₃ (99.5%, Sinopharm Chemical Reagent Co., Ltd.), were used after a pre-calcination at 800 °C to remove possible absorbed moisture or CO₂. Typically, for their synthesis, Sr_{0.82}Tb_{0.12}WO₄, SrCO₃ (2.62 mmol, 0.3870 g), Tb₄O₇ (0.10 mmol, 0.0717 g), and WO₃ (3.20 mmol, 0.7412 g) were homogenized using an agate mortar, followed by preheating at 800 °C for 10 h. The resultant powder was re-ground thoroughly by hand. Finally, it was heated at 1000 °C for another 15 h in air.

2.2. Characterizations

Powder XRD data were collected on a PANalytical X'pert diffractometer equipped with a PIXcel 1D detector (Cu K α radiation, 1.5406 Å). The operation voltage and current were 40 kV and 40 mA, respectively. Le Bail refinements were performed to obtain cell parameters using the TOPAS software package [24]. Scanning electron microscopy (SEM) was performed on an S4800 at an accelerating voltage of 10 kV. The elemental analysis was performed using SEM fitted with an INCAX-act energy dispersive spectrometer (EDS). Ultraviolet–visible diffuse reflectance spectrum (DRS) was recorded using a Shimadzu UV-3600 spectrometer equipped with an integrating sphere attachment. The analysis range was from 200 to 1200 nm, and BaSO₄ was used as the reflectance standard. Photoluminescence (PL) spectra were measured on a Hitachi F4600 fluorescence spectrometer at room temperature. The analysis range was from 450 to 600 nm, the excited wavelength was 250 nm, and the PL of the baseline was collected by using an empty glass cuvette.

2.3. Theoretical Calculations

Theoretical study on SrWO₄ was investigated via the Vienna Ab initio Simulation Package (VASP) [25]. The projector augmented-wave (PAW) method implemented in the VASP code was utilized to describe the interaction between the ionic cores and the valence electrons [26]. The generalized gradient approximation (GGA) parameterized by Perdew, Burke, and Ernzerhof (PBE) was employed to describe the exchange-correlation potential in standard density functional theory calculations [27]. For single point energy and density of states, a cutoff energy of 500 eV for the plane-wave basis and the 3 × 3 × 3 Monkhorst–Pack G-centered k -point meshes were employed.

2.4. Photocatalytic Performance Evaluation

Photocatalytic performances were tested on a gas-closed circulation system equipped with a vacuum device (LabSolar-IIIAG system, Perfect Light Ltd. Co.), a 150 mL Pyrex glass reactor, and a gas sampling port that was directly connected to a gas chromatograph (Shanghai Techcomp-GC7900,

TCD detector, molecular sieve 5A, N₂ gas carrier). In a typical run, 50 mg of catalyst was dispersed by a magnetic stirrer in 50 mL of 5 vol % TEOA aqueous solution. The solution was stirred, and a 10 °C cycling water bath was applied to keep the reaction vessel at a constant temperature. The light irradiation source was generated by an external 500W Hg lamp (CEL-M500, Beijing Au Light Ltd. Co.).

2.5. Preparation of the Cocatalysts

The loading of metal cocatalyst on photocatalyst was performed by a photodeposition method using the above setup [14]. For instance, 50 mg Sr_{0.82}Tb_{0.12}WO₄ sample, together with 1.0 mL of RuCl₃ (0.97 mg/mL), were mixed in 10 mL of distilled water. This solution was placed in a 150 mL Pyrex glass reactor with an ultrasonic treatment for 10 min, and then the mixture, in the presence of 5 vol % of TEOA, was irradiated using a 500 W high-pressure Hg lamp for 2 h. Finally, the powder sample was collected and washed with deionized water.

3. Results and Discussion

Figure 1 presents the whole XRD pattern of SrWO₄ with substantial doping of Tb³⁺, and the sharp peaks point to the high crystallinity of the as-prepared samples. For Sr_{1-1.5x}Tb_xWO₄ (0.00 ≤ x ≤ 0.20), it is evident that a pure phase of solid solutions was synthesized without any impurity peaks, when compared to the simulated XRD (ICSD-155793) of SrWO₄. The peak shift by Tb³⁺-doping is not obvious, but we can determine the change of the cell lattice parameters (*a*, *c*, and *V*) by Le Bail fitting of the whole powder XRD pattern [2,14]. The plot of *a*, *c*, and *V*, along with the increase in *x*, suggests a linear shrinkage (see Figure 2). These results evidently confirm that Tb³⁺ has been successfully incorporated into SrWO₄ without any structural change.

Scherrer's formula works best for the nanomaterials (1–100 nm), and the average crystallite sizes of SrWO₄ and Sr_{0.82}Tb_{0.12}WO₄ particles were estimated as per the following equation:

$$t = K\lambda/B\cos\theta_B, \quad (1)$$

where *t* is the crystallite size of the particle (assuming particles are spherical), *K* = 0.9, *λ* is the wavelength of X-ray radiation, *B* is the full width at half-maximum of the diffracted peak, and *θ_B* is the diffraction angle [28]. The estimated crystallite sizes based on the (011) peak for SrWO₄ and Sr_{0.82}Tb_{0.12}WO₄ are approximately 89.4 and 50.3 nm, respectively.

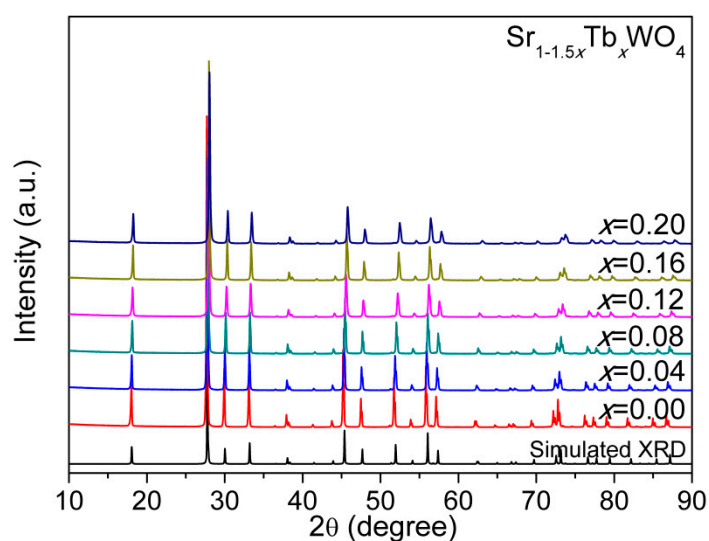


Figure 1. The XRD patterns for the Sr_{1-1.5x}Tb_xWO₄ (0 ≤ x ≤ 0.20), where the simulated XRD pattern for undoped SrWO₄ is also given.

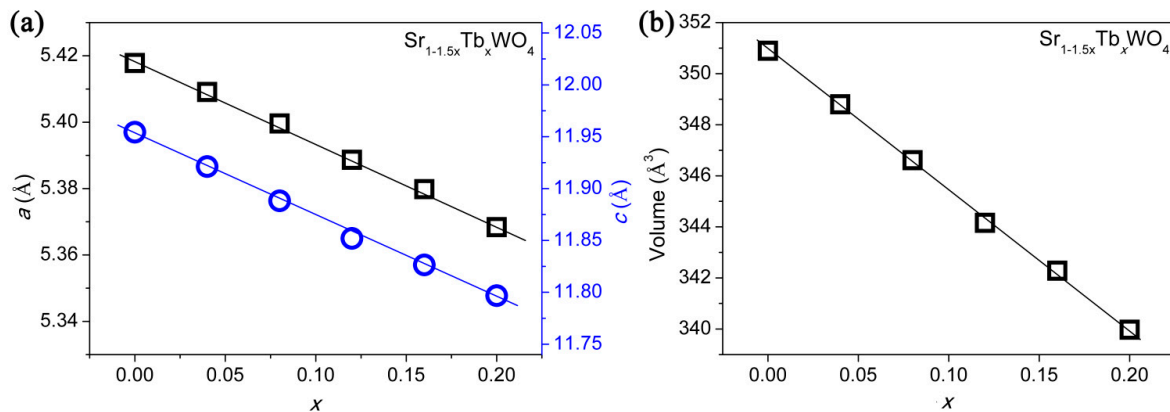


Figure 2. Estimated cell parameters for the $\text{Sr}_{1-1.5x}\text{Tb}_x\text{WO}_4$ ($0 \leq x \leq 0.20$) from Le Bail refinements on whole XRD patterns: (a) a and c , (b) volume.

The as-prepared solid solutions were observed by electron microscopy. Figure 3 shows the SEM images of nondoped SrWO_4 and $\text{Sr}_{0.82}\text{Tb}_{0.12}\text{WO}_4$ powders prepared under identical conditions. Both particles were well-crystallized, which is consistent with the XRD analysis. The particle size of $\text{Sr}_{0.82}\text{Tb}_{0.12}\text{WO}_4$ powder, 0.1–1 μm , was remarkably smaller than that of nondoped SrWO_4 powder, 1–2.4 μm . Since the SrWO_4 and $\text{Sr}_{0.82}\text{Tb}_{0.12}\text{WO}_4$ powders are bulk samples, the particle size determined by SEM is different from the particle size calculated by Scherrer's formula from XRD, but the relative size of the SrWO_4 and $\text{Sr}_{0.82}\text{Tb}_{0.12}\text{WO}_4$ powders were not changed. A sharp surface edge was observed for the La-doped SrWO_4 powder, whereas the surface of nondoped SrWO_4 was flat. The insert in Figure 3b shows an elemental analysis performed on the $\text{Sr}_{0.82}\text{Tb}_{0.12}\text{WO}_4$ sample, which gave an average atomic ratio of $\text{Sr/Tb/W/O} = 0.84:0.12:1.00:4.02$.

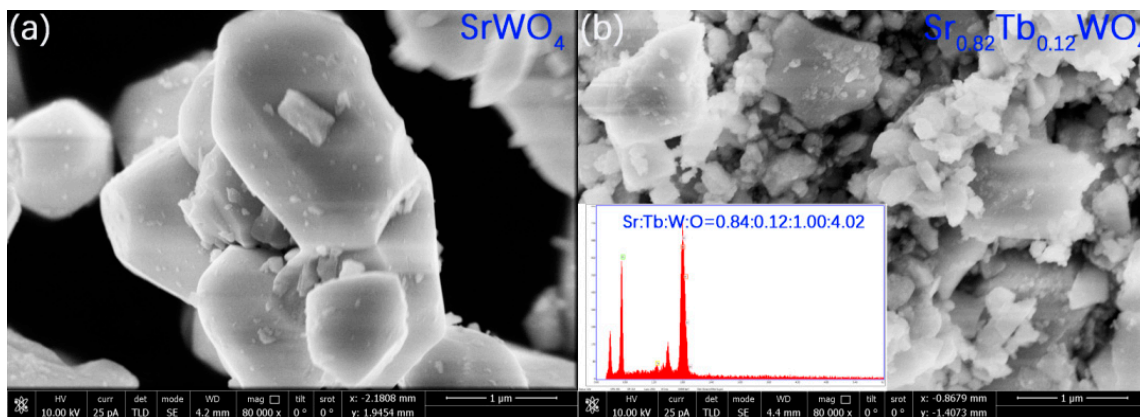


Figure 3. (a) SEM image for SrWO_4 . (b) SEM and EDS image for $\text{Sr}_{0.82}\text{Tb}_{0.12}\text{WO}_4$.

Figure 4a shows that the absorption band of SrWO_4 lies mainly in the UV region, and there is a steep edge which indicates that the absorption band is not due to the transition from impurity energy levels but from the bandgap transition [29]. For most semiconductors, the dependence of the absorption coefficient α on the bandgap energy E_g can be expressed by the following equation: $\alpha h\nu = A(h\nu - E_g)^{n/2}$, where h , ν , and A are the Planck constant, light frequency, and proportionality, respectively, and n is determined on the basis of the transition type (i.e., $n = 1$ for direct transition, $n = 4$ for indirect transition) [23]. The best fit of $(\alpha h\nu)^2$ vs. E_g was obtained only when n is 1, suggesting that direct transition across the energy bandgap of SrWO_4 is allowed (see Figure 4b). The extrapolated value of $h\nu$ at $\alpha = 0$ gives an absorption edge energy corresponding to E_g , which is 4.73 eV for SrWO_4 . Note that the reported value of the bandgap is in the range of 3.2–4.96 eV in the literature [16,18–21], where the difference comes from the different morphology of these samples.

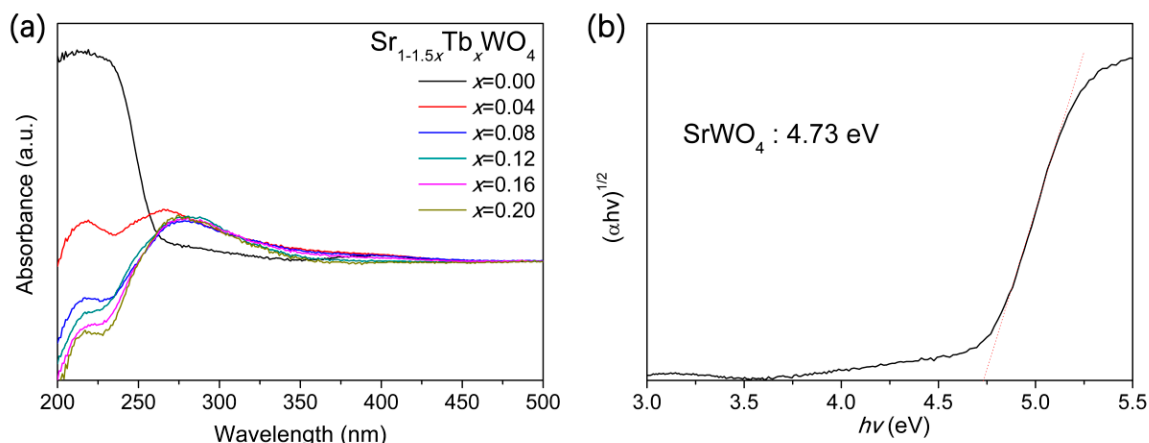


Figure 4. (a) UV-vis diffuse reflectance spectrum for $\text{Sr}_{1-1.5x}\text{Tb}_x\text{WO}_4$ solid solutions. (b) Estimated bandgap energy E_g with plot of $(\alpha hv)^2$ against photon energy (hv) for SrWO_4 .

As a result of the fluorescence phenomenon of $\text{Sr}_{1-1.5x}\text{Tb}_x\text{WO}_4$ solid solutions, the DRS patterns were interrupted at a range of 200~270 nm (see Figure 4a), in agreement with the excitation wavelength of excitation spectra patterns (see Figure 5a). However, we can conclude that the bandgaps of the Tb-doped samples are smaller than the nondoped SrWO_4 , because the light absorbance of the Tb-doped samples are obviously bigger than the nondoped samples at the wavelengths of 275~400 nm. Sometimes, the weak absorbance of photocatalyst could lead to a significant change of photocatalytic activity, such as Ni-doped InTaO_4 [2], and carbon dot-decorated C_3N_4 [30]. Nevertheless, in our work, the doped sample did not respond to simulated sunlight with 5 vol % TEOA solution. Figure 5a shows the photoluminescence emission spectra of the solid solutions by monitoring the Tb^{3+} emission at 250 nm. The change trends of emission intensity appeared as “volcano” types by increasing the Tb^{3+} content (see Figure 5b). The band-band PL phenomenon was monitored with the light energy approximately equal to the bandgap energy of the sample [31]. Usually, the recombination of photogenerated carriers and PL intensity are positively correlated in photocatalytic studies [32,33], and the photocatalytic activity related to the recombination of photogenerated electron and hole [34]. In other words, the weak PL intensity means that photoexcitation is difficult. The optimal sample regarding photoluminescence is $\text{Sr}_{0.82}\text{Tb}_{0.12}\text{WO}_4$, which means that the photogenerated electrons are easily excited from valence band to conduction band.

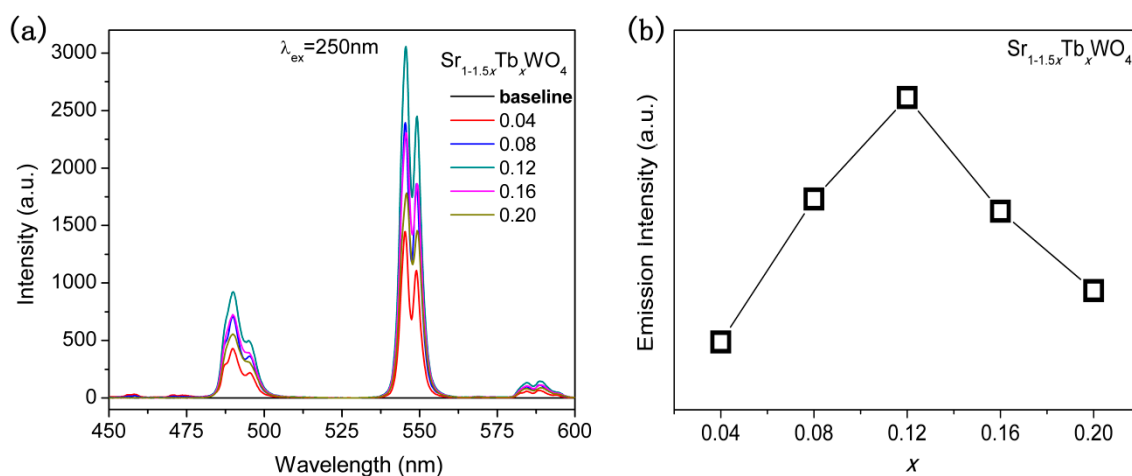


Figure 5. (a) The photoluminescence emission spectra of $\text{Sr}_{1-1.5x}\text{Tb}_x\text{WO}_4$ solid solutions by monitoring at 250 nm. (b) The emission intensity of the solid solutions against x .

To study the photocatalytic activity of SrWO_4 , the aqueous methanol and TEOA solutions were utilized as electron-donating sacrificial agents for H_2 evolution in our photocatalytic reactions. The H_2 evolution rate of SrWO_4 in 5 vol % aqueous TEOA is 2.1 times higher than it is in the 20 vol % aqueous methanol (see Figure 6). Furthermore, compared with the literature [22], the H_2 evolution rate of SrWO_4 is almost the same value as in aqueous methanol under UV light.

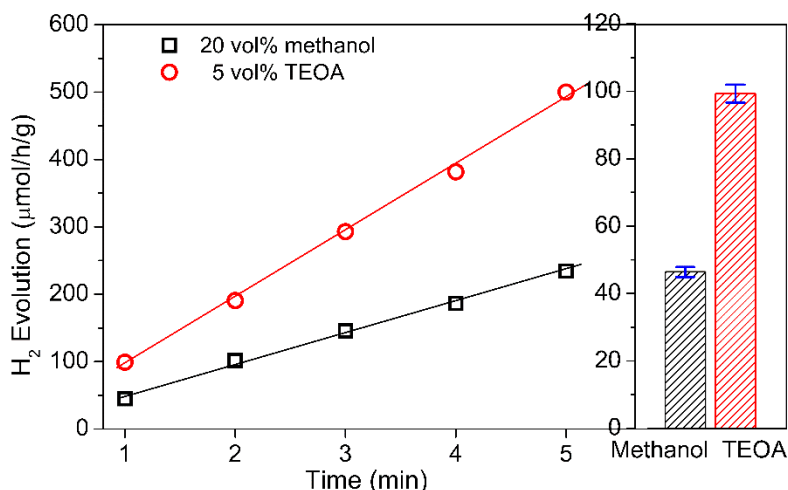


Figure 6. The H_2 evolution of SrWO_4 with different electron-donating sacrificial agents. Photocatalytic conditions: 50 mg SrWO_4 sample, 50 mL solution, 500 W Hg lamp.

The photocatalytic activity of the $\text{Sr}_{1-1.5x}\text{Tb}_x\text{WO}_4$ solid solutions toward the H_2 production at 5 h reaction times, in the presence of 5 vol % TEOA as electron-donating sacrificial agent under UV light, is shown in Figure 7. The H_2 production rates were changed by increasing the Tb^{3+} content in a trend of “volcano” type, which is in agreement with the photoluminescence emission intensity. Figure 7a shows that the optimum sample is $\text{Sr}_{0.82}\text{Tb}_{0.12}\text{WO}_4$, and that its H_2 evolution rate is $128.6 \mu\text{mol/h/g}$. Compared with the undoped SrWO_4 , the photocatalytic activity of $\text{Sr}_{0.82}\text{Tb}_{0.12}\text{WO}_4$ is improved about 1.3 times, which can be explained as follows: (1) The light absorption of the solid solutions are enhanced via the increasing of Tb^{3+} , leading to the improvement of photocatalytic activity [35]; (2) The non-equivalent doping of Tb^{3+} to replace Sr^{2+} in SrWO_4 can fabricate a metal vacancy in the bulk and surface of the material, which may constitute a recombination center [36]. Figure 7b shows that the H_2 evolution of the solid solutions is linear against time.

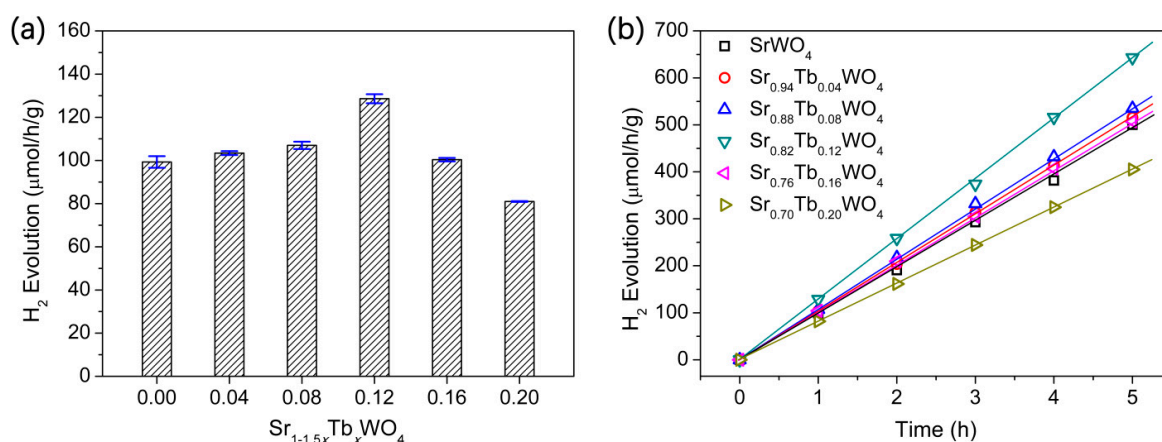


Figure 7. (a) The H_2 evolution rates of $\text{Sr}_{1-1.5x}\text{Tb}_x\text{WO}_4$ samples against increasing x . (b) The H_2 evolution of $\text{Sr}_{1-1.5x}\text{Tb}_x\text{WO}_4$ samples against time. Photocatalytic conditions: 50 mg photocatalyst, 50 mL 5% aqueous triethanolamine (TEOA) solution, 500 W Hg lamp.

The H₂ evolution rates of SrWO₄ micro/nanostructures were obviously improved by Pt- and Ru-cocatalysts [22]. Usually, metal cocatalysts offer photocatalytic water reduction sites, which means that photogenerated electrons prefer to move to metal cocatalysts [37,38]. In our experiment, the various cocatalysts, including Cu, Ag, Au, Pt, Ni, and Ru, were loaded onto the Sr_{0.82}Tb_{0.12}WO₄ sample to promote photocatalytic activity (Figure 8a). The Ru-cocatalyst loaded onto the photocatalysts had the optimum H₂ production rate (128.6 μmol/h/g), which is 1.3 times that of the nonloaded SrWO₄. Figure 8b shows that the H₂ evolution of the cocatalyst-loaded Sr_{0.82}Tb_{0.12}WO₄ samples is linear against time.

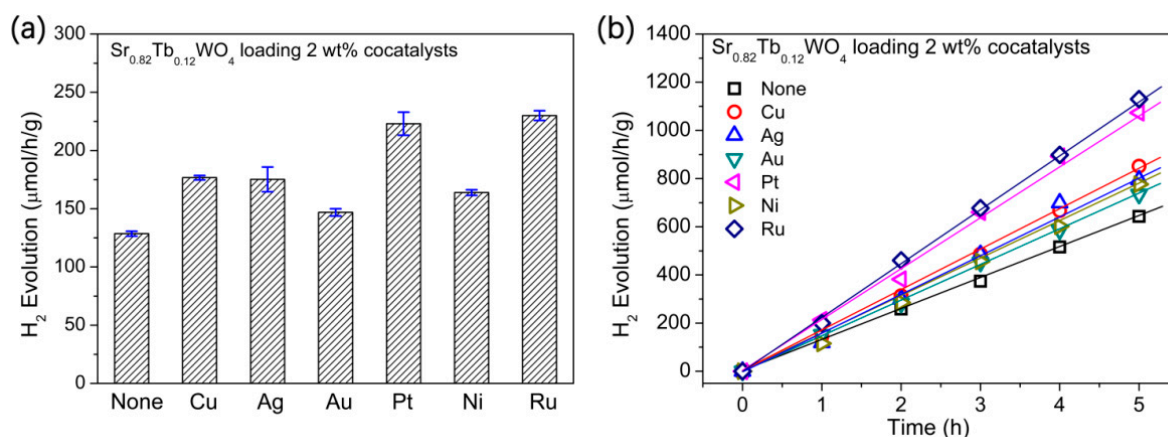


Figure 8. (a) The H₂ evolution rates of Sr_{0.82}Tb_{0.12}WO₄ samples with different cocatalysts. (b) The H₂ evolution of Sr_{0.82}Tb_{0.12}WO₄ samples against time. Photocatalytic conditions: 50 mg photocatalyst, 50 mL 5% TEOA solution, 500 W UV light.

The optimum usage of Ru-cocatalyst for the Sr_{0.82}Tb_{0.12}WO₄ sample was observed to be 1.5 wt % (Figure 9a). Its H₂ evolution rate was 281.9 μmol/h/g, which is 2.8 times that of the nonloaded SrWO₄. The photocatalytic activity of the optimum sample is stable after 30 h UV light irradiation, as shown in Figure 9b. In our work, the control experiments were performed without any sacrificial donor. However, the SrWO₄, Sr_{0.82}Tb_{0.12}, and 1.5 wt % Ru/Sr_{0.82}Tb_{0.12}WO₄ samples had no detectable photocatalytic activity in H₂ evolution. The XRD patterns of the as-prepared photocatalysts showed no obvious change before and after photocatalytic reaction (see Figure 10).

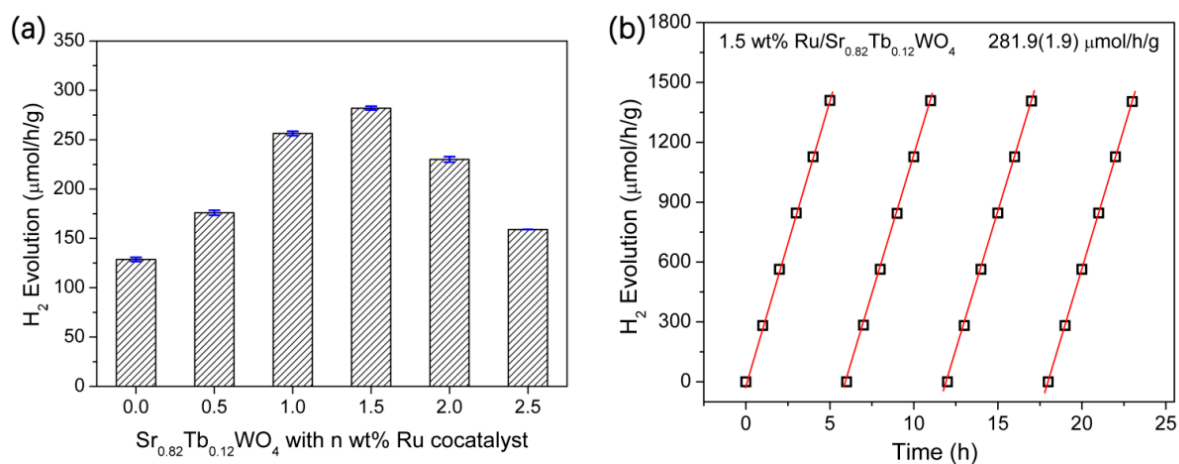


Figure 9. (a) The H₂ evolution rates of Sr_{0.82}Tb_{0.12}WO₄ solid solutions with differing amounts of cocatalyst. (b) A long-term photocatalytic reaction over Sr_{0.82}Tb_{0.12}WO₄ loaded with 1.5 wt % Ru-cocatalyst. Photocatalytic conditions: 50 mg photocatalyst, 50 mL 5% TEOA solution, 500 W Hg lamp.

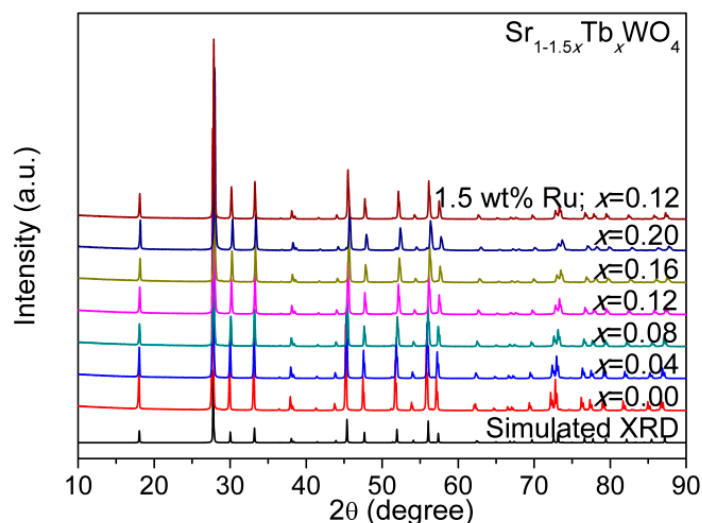


Figure 10. The XRD patterns of the solid solutions, and the recycled samples after photocatalysis.

In order to determine that the enhancement is really due to Tb or Ru for the optimum 1.5 wt % Ru-loaded $\text{Sr}_{0.82}\text{Tb}_{0.12}\text{WO}_4$ sample, we compared the photocatalytic H_2 evolution of SrWO_4 , 1.5 wt % Ru-loaded SrWO_4 , $\text{Sr}_{0.82}\text{Tb}_{0.12}\text{WO}_4$, and 1.5 wt % Ru-loaded $\text{Sr}_{0.82}\text{Tb}_{0.12}\text{WO}_4$ (see Table 1). Indeed, the value of [3]:[1] is larger than the value of [2]:[1], which means the doped Tb is better than the loaded Ru for H_2 evolution. The value of [4]:[2] is larger than [4]:[3], which indicates that the doped Tb is also better. Therefore, we can conclude that Tb is relatively more important for the H_2 evolution of SrWO_4 in our experiment.

Table 1. The photocatalytic H_2 evolution of four samples in 5 vol % TEOA under UV light.

Photocatalyst	[1] SrWO_4	[2] 1.5 wt % Ru-Loaded SrWO_4	[3] $\text{Sr}_{0.82}\text{Tb}_{0.12}\text{WO}_4$	[4] 1.5 wt % Ru-Loaded $\text{Sr}_{0.82}\text{Tb}_{0.12}\text{WO}_4$
H_2 evolution ($\mu\text{mol}/\text{h}/\text{g}$)	99.3	117.4	128.6	281.9
ratio		[2]:[1] = 1.18	[3]:[1] = 1.30	[4]:[1] = 2.84; [4]:[2] = 2.40; [4]:[3] = 2.19

To obtain further insight into the photocatalytic activity of SrWO_4 , the electronic structure of SrWO_4 was investigated by VASP calculations. Figure 11 shows the energy band dispersion and density of states (DOS). Although the bandgap (4.284 eV) from VASP calculations is usually underestimated, it nonetheless often provides important insight into the physicochemical behavior of the investigated materials [6,14]. The material is a direct bandgap semiconductor, as has been revealed from the DRS pattern. As shown in Figure 11a, both the valence band maximum and the conduction band minimum of SrWO_4 are located at the S point of the Brillouin zone, which explains the features of the measured DRS pattern, as does the reported literature [22]. This is in agreement with the inference from the DRS pattern. Both the lowly dispersive valence bands and the conduction bands should not be beneficial for the transport of the photoexcited electrons and holes. Their lowly dispersive bands, in turn, are likely to result in high recombination of electron hole pairs and, thus, account for the low photocatalytic activity of SrWO_4 . The total DOS shows that the bands of SrWO_4 can be classified into two parts (see Figure 11b). The top of the valence band is completely dominated by the O 2p orbital, while the bottom of the conduction band is mainly constituted by the W 5d orbital and the Sr 4d orbital. In addition, the band structure indicates that charge transfer upon photoexcitation occurs from the O 2p orbital to the empty W 5d orbital and Sr 4d orbital.

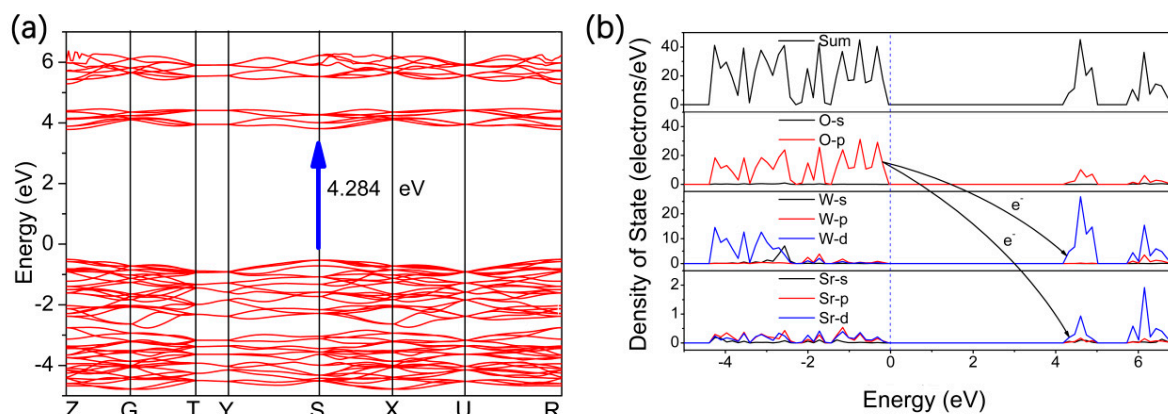


Figure 11. Theoretical calculations band structure and density of states for SrWO₄.

4. Conclusions

We prepared Sr_{1-1.5x}Tb_xWO₄ solid solutions by high-temperature solid state reaction. Le Bail fitting on powder XRD verified high purity and crystallinity of the as-prepared samples, and the SEM images showed that the SrWO₄ and Sr_{0.82}La_{0.12}WO₄ were composed of micron and submicron crystallites, respectively. DRS and theoretical calculations of SrWO₄ samples suggested a wide bandgap characteristic, which was 4.73 eV, assuming the direct semiconductor model. The valence band maximum was composed of O 2p orbitals, and the conduction band minimum was composed of both W 5d and Sr 4d orbitals. The H₂ evolution rates of SrWO₄ samples were 46.4 μmol/h/g and 99.3 μmol/h/g, with the 20 vol % methanol and 5 vol % TEOA aqueous solutions, respectively. The photocatalytic activity of SrWO₄ was improved by doping Tb³⁺ and then loading cocatalysts. The 1.5 wt % Ru-cocatalyst loaded onto Sr_{0.82}Tb_{0.12}WO₄ improved the H₂ evolution rate to 281.7 μmol/h/g. This photocatalyst remained stable and active even after five cycles (25 h in total). The improvement of photocatalytic performance for 1.5 wt % Ru/Sr_{0.82}Tb_{0.12}WO₄ was mainly due to the doped Tb in the crystal structure. These samples did not respond to simulated sunlight with the 5 vol % TEOA, and had no detectable photocatalytic activity in water under UV light. Our study demonstrates the photocatalytic H₂ evolution of Sr_{1-1.5x}Tb_xWO₄, and our preliminary attempt of Tb³⁺-doping and loading of various cocatalysts did, indeed, improve the activity. The next steps involve extending the studies to other rare earth ions to produce materials that absorb more of the visible region of the spectrum, or to complete the water-splitting reaction.

Author Contributions: Writing—Original Draft Preparation, J.Y. and X.S.; Writing—Review & Editing, J.Y. and J.S.; Supervision, T.Z.; Y.H.; Funding Acquisition, J.Y.

Funding: This research was funded by Science and Technology Project of Chongqing Municipal Education Commission (KJQN201801407) and Talent Introduction Project of Yangtze Normal University (2017KYQD22).

Acknowledgments: This work was financially supported by Science and Technology Project of Chongqing Municipal Education Commission (KJQN201801407), Talent Introduction Project of Yangtze Normal University (2017KYQD22).

Conflicts of Interest: The authors declare no conflict of interest.

References

1. Qi, J.; Zhang, W.; Cao, R. Solar-to-hydrogen energy conversion based on water splitting. *Adv. Energy Mater.* **2018**, *8*, 1–16. [[CrossRef](#)]
2. Zou, Z.G.; Ye, J.H.; Sayama, K.; Arakawa, H. Direct splitting of water under visible light irradiation with an oxide semiconductor photocatalyst. *Nature* **2001**, *414*, 625–627.
3. Shen, S.L.; Wang, Q.B. Rational tuning the optical properties of metal sulfide nanocrystals and their applications. *Chem. Mater.* **2013**, *25*, 1166–1178. [[CrossRef](#)]

4. Ahmed, M.; Guo, X.X. A review of metal oxynitrides for photocatalysis. *Inorg. Chem. Front.* **2016**, *3*, 578–590. [[CrossRef](#)]
5. Yang, J.; Xie, T.P.; Liu, C.L.; Xu, L.J. Facile fabrication of dumbbell-like beta-Bi₂O₃/graphene nanocomposites and their highly efficient photocatalytic activity. *Materials* **2018**, *11*, 1359. [[CrossRef](#)]
6. Yang, J.; Fu, H.; Yang, D.F.; Gao, W.L.; Cong, R.H.; Yang, T. ZnGa_{2-x}In_xS₄ (0 ≤ x ≤ 0.4) and Zn_{1-2y}(CuGa)_yGa_{1.7}In_{0.3}S₄ (0.1 ≤ y ≤ 0.2): Optimize visible light photocatalytic H₂ evolution by fine modulation of band structures. *Inorg. Chem.* **2015**, *54*, 2467–2473.
7. Yan, H.J.; Yang, J.H.; Ma, G.J.; Wu, G.P.; Zong, X.; Lei, Z.B.; Shi, J.Y.; Li, C. Visible-light-driven hydrogen production with extremely high quantum efficiency on Pt-PdS/CdS photocatalyst. *J. Catal.* **2009**, *266*, 165–168. [[CrossRef](#)]
8. Pan, C.S.; Takata, T.; Nakabayashi, M.; Matsumoto, T.; Shibata, N.; Ikuhara, Y.; Domen, K. A complex perovskite-type oxynitride: The first photocatalyst for water splitting operable at up to 600 nm. *Angew. Chem. Int. Ed.* **2015**, *54*, 2955–2959. [[CrossRef](#)] [[PubMed](#)]
9. Maeda, K.; Teramura, K.; Saito, N.; Inoue, Y.; Domen, K. Improvement of photocatalytic activity of (Ga_{1-x}Zn_x)(N_{1-x}O_x) solid solution for overall water splitting by co-loading Cr and another transition metal. *J. Catal.* **2006**, *243*, 303–308. [[CrossRef](#)]
10. Cui, C.; Li, S.; Qiu, Y.W.; Hu, H.H.; Li, X.Y.; Li, C.R.; Gao, J.K.; Tang, W.H. Fast assembly of Ag₃PO₄ nanoparticles within three-dimensional graphene aerogels for efficient photocatalytic oxygen evolution from water splitting under visible light. *Appl. Catal. B-Environ.* **2017**, *200*, 666–672. [[CrossRef](#)]
11. Yang, H.X.; Liu, X.Y.; Sun, S.N.; Nie, Y.; Wu, H.P.; Yang, T.Y.; Zheng, S.J.; Lin, S.L. Green and facile synthesis of graphene nanosheets/K₃PW₁₂O₄₀ nanocomposites with enhanced photocatalytic activities. *Mater. Res. Bull.* **2016**, *78*, 112–118. [[CrossRef](#)]
12. Zhang, N.; Yang, M.Q.; Liu, S.Q.; Sun, Y.G.; Xu, Y.J. Waltzing with the Versatile Platform of Graphene to Synthesize Composite Photocatalysts. *Chem. Rev.* **2015**, *115*, 10307–10377. [[CrossRef](#)]
13. Wang, G.J.; Jing, Y.; Ju, J.; Yang, D.F.; Yang, J.; Gao, W.L.; Cong, R.H.; Yang, T. Ga₄B₂O₉: An efficient borate photocatalyst for overall water splitting without cocatalyst. *Inorg. Chem.* **2015**, *54*, 2945–2949. [[CrossRef](#)]
14. Yang, J.; Jiang, P.F.; Yue, M.F.; Yang, D.F.; Cong, R.H.; Gao, W.L.; Yang, T. Bi₂Ga₄O₉: An undoped single-phase photocatalyst for overall water splitting under visible light. *J. Catal.* **2017**, *345*, 236–244. [[CrossRef](#)]
15. Zheng, Y.H.; Lin, J.T.; Wang, Q.M. Emissions and photocatalytic selectivity of SrWO₄:Ln³⁺ (Eu³⁺, Tb³⁺, Sm³⁺ and Dy³⁺) prepared by a supersonic microwave co-assistance method. *Photochem. Photobiol. Sci.* **2012**, *11*, 1567–1574. [[CrossRef](#)]
16. Shan, Z.C.; Wang, Y.M.; Ding, H.M.; Huang, F.Q. Structure-dependent photocatalytic activities of MWO₄ (M = Ca, Sr, Ba). *J. Mol. Catal. A-Chem.* **2009**, *302*, 54–58. [[CrossRef](#)]
17. Cavalcante, L.S.; Sczancoski, J.C.; Batista, N.C.; Longo, E.; Varela, J.A.; Orlandi, M.O. Growth mechanism and photocatalytic properties of SrWO₄ microcrystals synthesized by injection of ions into a hot aqueous solution. *Adv. Powder. Technol.* **2013**, *24*, 344–353. [[CrossRef](#)]
18. Shivakumara, C.; Saraf, R.; Behera, S.; Dhananjaya, N.; Nagabhushana, H. Scheelite-type MWO₄ (M = Ca, Sr, and Ba) nanophosphors: Facile synthesis, structural characterization, photoluminescence, and photocatalytic properties. *Mater. Res. Bull.* **2015**, *61*, 422–432. [[CrossRef](#)]
19. Liu, X.Y.; Nie, Y.; Yang, H.X.; Sun, S.N.; Chen, Y.Y.; Yang, T.Y.; Lin, S.L. Enhancement of the photocatalytic activity and electrochemical property of graphene-SrWO₄ nanocomposite. *Solid State Sci.* **2016**, *55*, 130–137. [[CrossRef](#)]
20. Talebi, R.; Safari, A. Synthesis, characterization, and investigation magnetic and photocatalytic property of SrWO₄ nanoparticles. *J. Mater. Sci-Mater. El.* **2016**, *27*, 9842–9846. [[CrossRef](#)]
21. Sahmi, A.; Bensadok, K.; Zirour, H.; Trari, M. Physical and photoelectrochemical characterizations of SrWO₄ prepared by thermal decomposition: Application to the photo electro-oxidation of ibuprofen. *J. Solid State Electr.* **2017**, *21*, 2817–2824. [[CrossRef](#)]
22. Chen, D.; Liu, Z.; Ouyang, S.X.; Ye, J.H. Simple room-temperature mineralization method to SrWO₄ micro/nanostructures and their photocatalytic properties. *J. Phys. Chem. C.* **2011**, *115*, 15778–15784. [[CrossRef](#)]
23. Yang, J.; Yue, M.F.; Ju, J.; Cong, R.H.; Gao, W.L.; Yang, T. Co-molten solvothermal method for synthesizing chalcopyrite CuFe_{1-x}CrxS₂ (x ≤ 0.4): High photocatalytic activity for the reduction of nitrate ions. *Dalton Trans.* **2014**, *43*, 15385–15390.

24. TOPAS, V4. 1-beta, Bruker AXS, Karlsruhe, Germany. 2004. Available online: <https://www.bruker.com/products/x-ray-diffraction-and-elemental-analysis/x-ray-diffraction/xrd-software/topas.html> (accessed on 7 May 2019).
25. Kresse, G.; Furthmüller, J. Efficient iterative schemes for ab initio total-energy calculations using a plane-wave basis set. *Phys. Rev. B* **1996**, *54*, 11169–11186. [[CrossRef](#)]
26. Blochl, P.E. Projector augmented-wave method. *Phys. Rev. B* **1994**, *50*, 17953–17979. [[CrossRef](#)]
27. Perdew, J.P.; Burke, K.; Ernzerhof, M. Generalized gradient approximation made simple. *Phys. Rev. Lett.* **1996**, *77*, 3865–3868. [[CrossRef](#)]
28. Huang, X.; Jing, Y.; Yang, J.; Ju, J.; Cong, R.H.; Gao, W.L.; Yang, T. Flower-like nanostructure $M\text{Nb}_2\text{O}_6$ ($M = \text{Mn}, \text{Zn}$) with high surface area: Hydrothermal synthesis and enhanced photocatalytic performance. *Mater. Res. Bull.* **2014**, *51*, 271–276. [[CrossRef](#)]
29. Jing, D.; Guo, L. A novel method for the preparation of a highly stable and active CdS photocatalyst with a special surface nanostructure. *J. Phys. Chem. B* **2006**, *110*, 11139–11145. [[CrossRef](#)]
30. Liu, J.; Liu, Y.; Liu, N.Y.; Han, Y.Z.; Zhang, X.; Huang, H.; Lifshitz, Y.; Lee, S.T.; Zhong, J.; Kang, Z.H. Metal-free efficient photocatalyst for stable visible water splitting via a two-electron pathway. *Science* **2015**, *347*, 970–974. [[CrossRef](#)]
31. Nayak, S.; Mohapatra, L.; Parida, K. Visible light-driven novel g- $\text{C}_3\text{N}_4/\text{NiFe-LDH}$ composite photocatalyst with enhanced photocatalytic activity towards water oxidation and reduction reaction. *J. Mater. Chem. A* **2015**, *3*, 18622–18635. [[CrossRef](#)]
32. Zhang, Y.; Gu, J.; Murugananthan, M.; Zhang, Y.R. Development of novel $\alpha\text{-Fe}_2\text{O}_3/\text{NiTiO}_3$ heterojunction nanofibers material with enhanced visible-light photocatalytic performance. *J. Alloy. Comp.* **2015**, *630*, 110–116. [[CrossRef](#)]
33. Tan, L.L.; Ong, W.J.; Chai, S.P.; Mohamed, A.R. Noble metal modified reduced graphene oxide/ TiO_2 ternary nanostructures for efficient visible-light-driven photoreduction of carbon dioxide into methane. *Appl. Catal. B: Environ.* **2015**, *166–167*, 251–259. [[CrossRef](#)]
34. Kudo, A.; Miseki, Y. Heterogeneous photocatalyst materials for water splitting. *Chem. Soc. Rev.* **2009**, *38*, 253–278. [[CrossRef](#)]
35. Ni, L.; Tanabe, M.; Irie, H. A visible-light-induced overall water-splitting photocatalyst: Conduction-band-controlled silver tantalate. *Chem. Commun.* **2013**, *49*, 10094–10096. [[CrossRef](#)]
36. Zou, Z.G.; Ye, J.H.; Arakawa, H. Photocatalytic behavior of a new series of $\text{In}_{0.8}\text{M}_{0.2}\text{TaO}_4$ ($M = \text{Ni}, \text{Cu}, \text{Fe}$) photocatalysts in aqueous solutions. *Catal. Lett.* **2001**, *75*, 3–4. [[CrossRef](#)]
37. Ran, J.R.; Zhang, J.; Yu, J.G.; Jaroniec, M.; Qiao, S.Z. Earth-abundant cocatalysts for semiconductor based photocatalytic water splitting. *Chem. Soc. Rev.* **2014**, *43*, 7787–7812. [[CrossRef](#)]
38. Ma, B.; Cong, R.H.; Gao, W.L.; Yang, T. Photocatalytic overall water splitting over an open-framework galliumborate loaded with various cocatalysts. *Catal. Commun.* **2015**, *71*, 17–20. [[CrossRef](#)]

